ACS OMEGA

http://pubs.acs.org/journal/acsodf

Article

Low Friction of Graphene Oxide Aggregates in Lubricant Oil between a Steel Ball and Glass Disk under Boundary Lubrication

Hiroshi Kinoshita,* Tatsuya Okamoto, Yutaro Hirai, Koichi Sugano, and Matsumoto Naohiro

Cite This: *ACS Omega* 2022, 7, 40983−40989

Read Online

ACCESS | Metrics & More | Article Recommendations | Supporting Information

ABSTRACT: Previously, isolated nanocarbons in lubricating oils were considered essential for good lubrication. However, we observed that graphene oxide (GO) aggregates in lubricating oil have lower frictional properties than isolated dispersed GO. The GO was dispersed in polyα-olefin (PAO) using alkylamine at different ratios of GO and alkylamine, or it was heated at different temperatures to synthesize high- and low-dispersible GO-dispersed PAO. X-ray photoelectron spectroscopy (XPS), Fourier transform infrared spectroscopy (FTIR), and Raman spectroscopy measurements showed that low-dispersible modified GOs retained many of the original GO chemical and structural features. Macrotribological tests between a steel ball and glass disk in GO-dispersed oil were conducted with a load of 5 N under boundary lubrication. The friction interface was observed in situ using an optical microscope. In the low-dispersible GO-dispersed PAO, many GO aggregates were observed through optical microscopy. Surprisingly, the friction coefficients decreased when the GO aggregates entered the friction interface and covered the contact area. The low-dispersible GO-dispersed PAO using alkylamine had the lowest friction coefficient of 0.05, as the GO aggregates covered the contact area. From microtribological tests with a load of 0.8 mN as well, it is assumed that the low friction of the GO aggregates originates due to the sliding between the weakest shear layers in the aligned multiple GO layers.

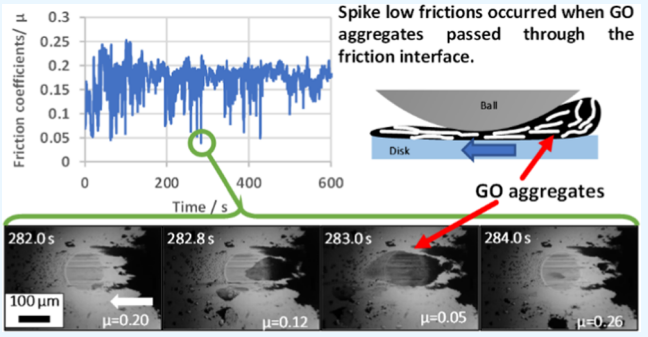

1. INTRODUCTION

Many researchers have investigated the tribological properties of graphene oxide (GOs) as additives in water and lubrication oil.[1−14] Although the size of the GO can exceed 10 μm, its thickness is less than 1 nm. Thus, it is considered to enter narrow friction interfaces under boundary lubrication. The numerous oxygen functional groups (polar groups) of GO[15] facilitate its dissolution in polar liquids.[16] However, its dispersal is difficult in low-polar liquids such as lubricating oil. Moreover, the large surface area of nanoparticles, including GO, exacerbates aggregation, which is a major problem for additives in lubricant oils. Aggregation reduces the effective particle concentration and prevents nanoparticles from entering the friction interfaces. Many research efforts have been directed toward producing stable well-dispersed additives,[17] and many previous studies using GO have concluded that high-dispersible GO-dispersed oil is better for low friction.[1,5,8−10]

However, we observed a low friction effect of GO aggregates in the GO water dispersion.[18] We conducted in situ observations of the friction interface between a SUJ2 ball and soda-lime glass disk in a GO water dispersion using optical microscopy. GO aggregates were formed by their accumulation in front of the contact area between the ball and the disk. When the aggregates entered the contact area, they prevented direct contact between the ball and disk, which lowered the friction. In addition, carbon nanotube aggregates in lubricating oil were observed to increase the oil film thickness and lower friction in mixed and hydrodynamic lubrication.[19]

In this study, GO was dispersed in poly α-olefin (PAO) using dispersants or heating. High- or low-dispersible GO-dispersed PAOs were synthesized under various conditions. Analyses of the samples were conducted using X-ray photoelectron spectroscopy (XPS), Fourier transform infrared spectroscopy (FTIR), and Raman spectroscopy. The friction tests between the steel ball and glass disk in the GO-dispersed PAO were conducted with a load of 5 N using a ball-on-disk-type tribometer. In addition, a ball-on-plate-type microtribometer was used with a microNewton load (0.8 mN) for mild friction. In situ friction interface observations were performed using optical microscopy in both tribometers.

Received: July 3, 2022
Accepted: October 26, 2022
Published: November 4, 2022

2. EXPERIMENTAL SECTION

GO was synthesized using the modified Hummers' method. The synthesis methods for GO have been described in previous studies.[14] PAO, with a viscosity of 14.5 mPa s at 40 °C, was used as the lubricating oil. To disperse GO (polar molecules) in PAO (nonpolar molecules), the degree of oxidation of GO should be decreased. Two methods were used in this study, using a dispersant (alkylamine) and heating the GO. In this study, oleylamine was used as alkylamine for the dispersant. In the GO water dispersion method, GO and alkylamine were mixed in mass ratios of 1:1, 1:4, and 1:10, filtered, heated to remove water, and then dispersed in PAO (referred to as GOA1, GOA4, and GOA10, respectively). GO was heated at 130, 200, and 250 °C and dispersed in PAO (referred to as GOT130, GOT200, and GOT250, respectively). All GO-dispersed PAOs underwent ultrasonication for 1 h.

For analyses using XPS, FTIR, and Raman spectroscopy, dried GOs were prepared by dropping as-synthesized GO water dispersions on silicon wafers, and dried GOT130, GOT200, and GOT250 were obtained by heating the dried GOs at 130, 200, and 250 °C, respectively, in air. In addition, dried GOA1, GOA4, and GOA10 particles were prepared before dispersing in PAO. The concentration of GO in all GO-dispersed PAOs was 1 mass % at the macro-load tests and 10 mass % at the micro-load tests.

Figure 1a shows the schematic of the tribometer for N-level loads using an optical microscope. A JIS−SUJ2 steel ball with a diameter of 10 mm was slid against a soda-lime glass disk with a load of 5 N. The ball was fixed and did not rotate. The sliding speed was set at 1 mm/s. The in situ observations of the friction interfaces revealed that when no GO aggregates existed in the friction interfaces, ball surfaces directly contacted disk surfaces. This indicates that the macrotribological tests were performed under boundary lubrication. The Young's modulus and surface roughness R_a of the soda-lime glass disk were 72 GPa and 11 nm, respectively. The Young's modulus of the SUJ2 ball is 207 GPa. The maximum Hertzian contact pressure was calculated as 501 MPa for the load of 5 N. The frictional interfaces were photographed using an optical microscope (×200, 25 fps). A white light-emitting diode (LED) was used as the light source.

Figure 1b shows a schematic of the microtribometer with an optical microscope for mN-level loads. The microtribometer used in this study, which is the same force measurement system used in conventional atomic force microscopy (AFM), has a cantilever and an optical lever system to measure the adhesion and friction forces. The ball is attached to the cantilever, and the glass plate is horizontally moved for friction and vertically for load using amplified piezoelectric (PZT) actuators. The load, sliding width, sliding frequency, and sliding speed are 0.8 mN, 200 μm, 10 s, and 20 μm/s, respectively. Microtribological tests were also performed under boundary lubrication. The calculated maximum Hertzian contact pressure for a load of 0.8 mN was 126 MPa.

The disks and balls were cleaned by ultrasonication in acetone, ethanol, and water for 5 min each. The tests were conducted at least five times under identical conditions.

3. RESULTS AND DISCUSSION

Figure 2 shows the photographs of the GO-dispersed PAO with a concentration of 1 mass % taken immediately (top) and a month after dispersion (bottom). All GO-dispersed PAO appeared to be well dispersed. GOA10 and GOT250 exhibit long-term stability and high dispersibility. Although GOA3 and GOT200 were just precipitated only slightly, they also exhibited high dispersibility. However, GOA1 and GOT130 precipitated and exhibited low dispersibility. GOA1 and

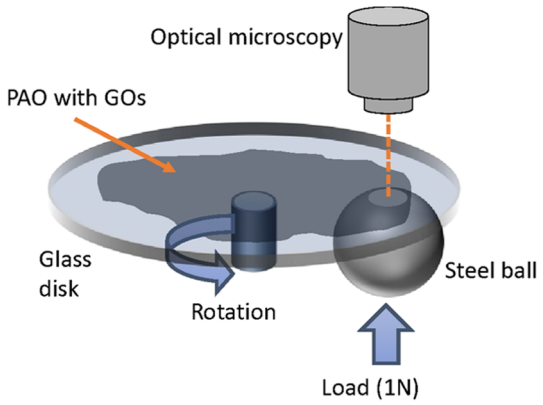

(a) Tribometer for N level loads with optical microscope

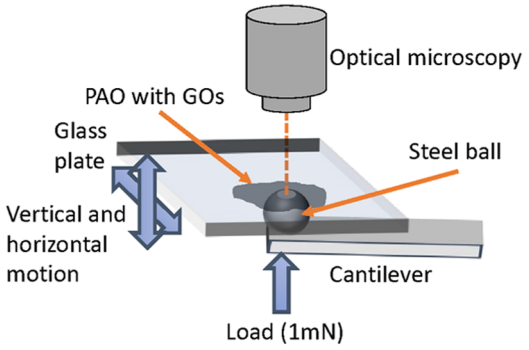

(b) Microtribometer for mN level loads with optical microscope

Figure 1. Schematic representation of the tribometers used in this study. (a) Tribometer for the N-level loads with an optical microscope. (b) Microtribometer for the mN-level loads with an optical microscope.

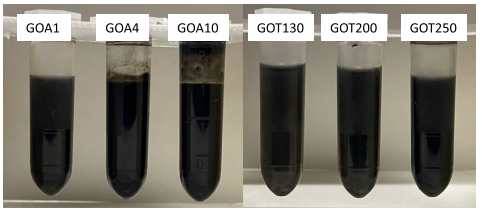

(a) Immediately after dispersion

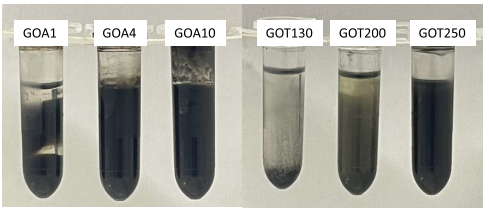

(b) One month after dispersion

Figure 2. Photos of the GO-dispersed PAO (a) immediately after dispersion and (b) 1 month after dispersion.

https://doi.org/10.1021/acsomega.2c04181
ACS Omega 2022, 7, 40983−40989

GOT130 were dispersed between two slide glasses, and the size of the GO aggregates was measured by optical microscopy. The sizes of the GO aggregates for GOA1 and GOT130 were mainly distributed from 5 to 50 μm and from 1 to 20 μm, respectively. Sometimes the sizes reached 100 μm for GOA1 and 50 μm for GOT130.

The C 1s spectra of the GO, GOA1, and GOT130 measured by XPS are shown in Figure 3. The C 1s spectra of GOA4, GOA10, GOT200, and GOT250 are shown in Figure S1. No N 1s peaks were detected in any of the samples. The C 1s spectrum of the as-synthesized GO contains C−C (284.6 eV) and oxygen functional groups of C−O (285.7 eV), C═O (287.0 eV), and O−C═O (288.8 eV).[20] The C 1s spectra of the GOA1 and GOT130 have high peaks, while GOA4, GOA10, GOT200, and GOT250 have smaller peaks for the oxygen functional groups compared to those of GO, GOA1, and GOT130. The O/C atomic ratios of all of the samples were measured by the areas of the peaks in the C 1s spectra, as shown in Figure 3d. An increase in the amount of alkylamine gradually decreased the O/C ratios. The O/C ratios of GOT200 and GOT250 were half that of GOT130. The XPS spectra indicated that the reductions in GOA1 and GOT130 were lower than those of GOA4, GOA10, GOT200, and GOT250 and had many oxygen functional groups.

The FTIR spectra of GO, GOA1, and GOT130 are shown in Figure 4. The peaks at 1729, 1631, 1382, and 1072 cm^{-1} were attributed to the vibrations of C═O, C═C / H_2O, O−H, and C−O.[21] The peak at 1433 cm^{-1} originates from the vibration of C−H,[22] and those at 2923 and 2851 cm^{-1} indicate vibrations of sp^3 C−H.[23] A broad peak around 3200 cm^{-1} was attributed to the vibration of O−H.[22,24−26] The FTIR spectra of GO and GOA1 were almost identical. Although the peaks at 2923 and 2851 cm^{-1} in the FTIR spectrum of GOT130 were lower than those of the GO, the FTIR spectra of GO and GOT130 were very similar. The FTIR spectra of GOA4, GOA10, GOT200, and GOT250 are shown in Figure S2. Decreases in the C═O (1729), O−H (1382), and C−O (1072) peaks were observed in the FTIR spectra of GOA4 and GOA10. The FTIR spectra of GOT200 and GOT250 showed decreased peaks of C═O (1729 cm^{-1}), O−H(1382 cm^{-1}), and sp^3 C−H(2923 and 2851 cm^{-1}), and broad peaks of O−H (around 3200 cm^{-1}). The FTIR spectra also show that the reductions of GOA1 and GOT130 were weak, and they also retained the oxygen functional groups of GO.

Figure 5 shows the Raman spectra of GO, GOA1, and GOT130, whose features are almost identical to each other. The spectra have G (around 1600 cm^{-1}) and D (around 1350 cm^{-1}) bands. The intensity ratios of the G and D bands (I_D/I_G) of GO, GOA1, and GOT130 are also shown in Figure 5. The Raman spectra and I_D/I_G of GOA4, GOA10, GOT200, and GOT250 are also displayed in Figure S3. The I_D/I_G ratios of all of the spectra were almost identical. This means that the alkylamine modification and heating treatments in this study did not change the structural features.[21]

The XPS, FTIR, and Raman measurements indicate that the reductions of GOA1 and GOT130 are weaker than those of GOA4, GOA10, GOT200, and GOT250, and they have a large concentration of oxygen functional groups. It is concluded that GOA1 and GOT130 retain the chemical and structural features of GO much better than GOA4, GOA10, GOT200, and GOT250.

Figure 6 shows the friction coefficients of GOA4, GOA10, GOT200, GOT250, and pure PAO as functions of the friction

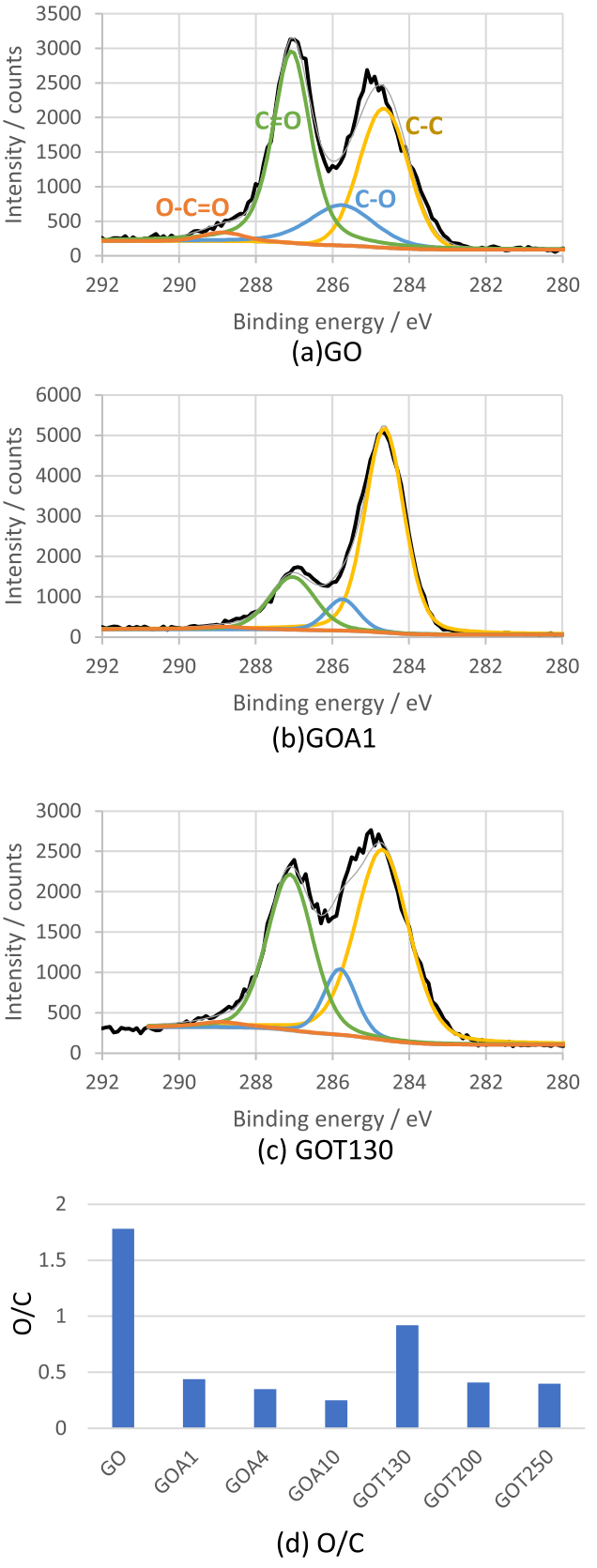

Figure 3. C 1s spectra of (a) GO, (b) GOA1, and (c) GOT130 measured by XPS, and (d) the O/C ratios of all samples.

time. The friction coefficients of these high-dispersible GO-dispersed PAO were approximately between 0.1 and 0.2, while the GO-dispersed PAO prepared using the heating method

https://doi.org/10.1021/acsomega.2c04181
ACS Omega 2022, 7, 40983−40989

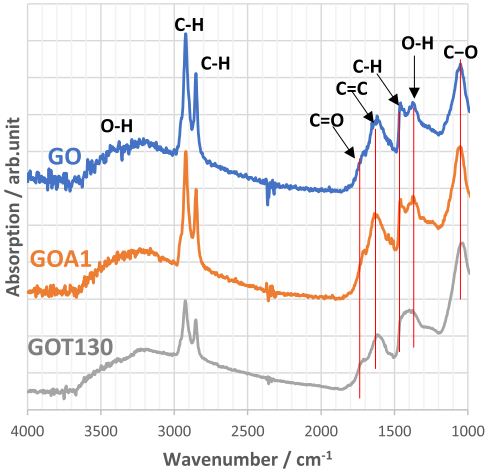

Figure 4. FTIR spectra of GO, GOA1, and GOT130.

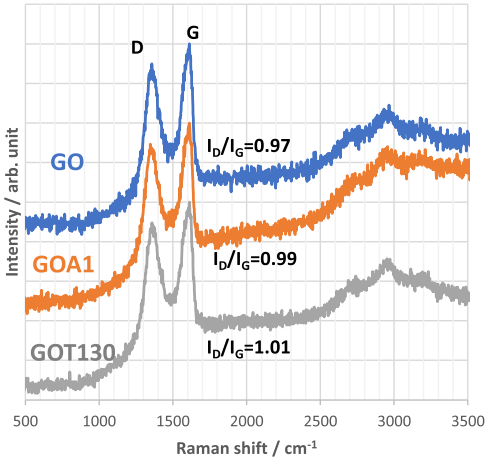

Figure 5. Raman spectra of GO, GOA1, and GOT130.

tended to have a higher coefficient. The friction coefficients of the high-dispersible GO-dispersed PAO were lower than those of the pure PAO. In situ observations using GOA4, GOA10, GOT200, and GOT250, which are shown in Figure S4, revealed that small GO aggregates with sizes less than 5 μm existed around the frictional interface (the image of GOA10 is the most obvious). Although these small GO aggregates sometimes passed through the friction interface, the friction did not change. It was considered that the GO and the much small GO aggregates, which were too small to be observed with the optical microscope, would enter the friction interface, prevent direct contact between the ball and disk surfaces, and thereby reduce the friction.

Figure 7 shows the friction coefficients as a function of the friction time with GOA1 and GOT130, which had low dispersibility. The friction coefficient of GOA1 exceeded 0.15 multiple times. However, sometimes it rapidly decreased. Some friction coefficients of the low-spike frictions of GOA1 were below 0.05. These low-spike frictions were also observed for GOT130 as well. Representative low-spike friction values are indicated by red circles in Figure 7. The friction coefficient of GOT130 during low-spike friction was approximately 0.1.

In situ observations using GOA1 and GOT130 revealed that many GO aggregates with sizes of more than 50 μm existed, which arose from the high concentrations of the oxygen functional groups. Figure 8 shows the optical microscope images and the friction coefficient and displacement between the ball and disk surfaces when the GO aggregates of GOA1 passed through the friction interface (friction time ranged from 282.0−284.0 s). The disk moved from the right to the left in the optical microscope images. The displacement between the ball and disk surfaces was calculated using the interference fringes. The black substance at the front of the friction interfaces comprised accumulated GO aggregates. At 282.0 s, no GO aggregates were observed in the friction interface, and the friction coefficient was 0.20. At 282.8 s, half the GO aggregates passed through the friction interface, and the friction coefficient decreased to 0.15. The observed GO aggregates were newly flowing and not from the accumulation at the front of the friction interface. At 283.0 s, the friction interface was completely covered by the GO aggregates, which were pushed out and widened by the high pressure and shear force of friction, with the lowest friction coefficient value of

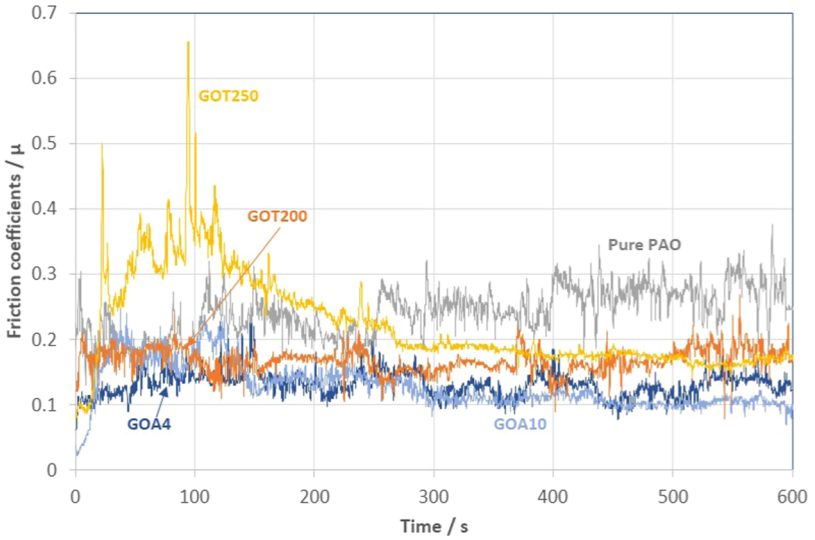

Figure 6. Friction coefficients as a function of the friction time using GOA4, GOA10, GOT200, GOT250 (high-dispersible GO-dispersed PAO), and pure PAO.

https://doi.org/10.1021/acsomega.2c04181
ACS Omega 2022, 7, 40983−40989

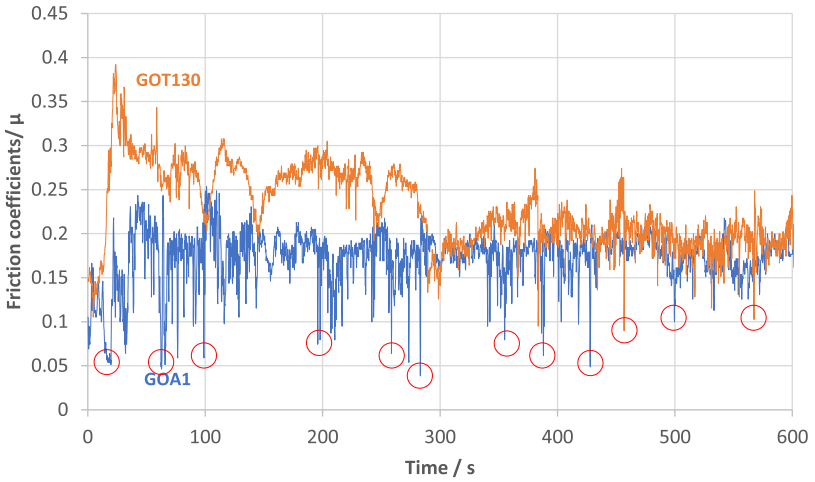

Figure 7. Friction coefficients as a function of the friction time using GOA1 and GOT130 (low-dispersible GO-dispersed PAO). Representative low-spike frictions are indicated by the red circles.

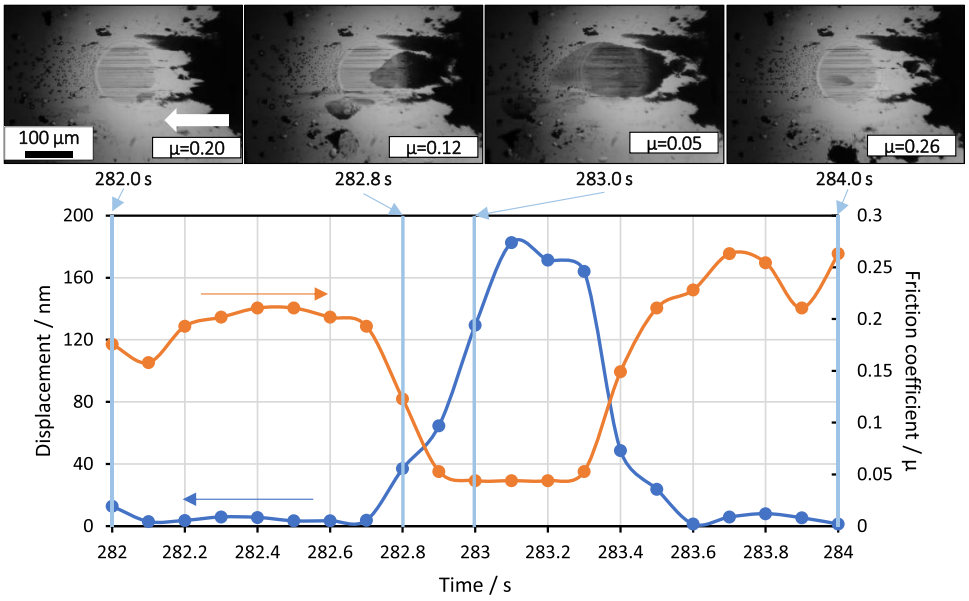

Figure 8. Optical microscope images (upper graphs) and friction coefficient and displacement between the ball and disk surfaces (lower graphs) when the GO aggregates of GOA1 passed through the friction interface. The arrow in the optical microscope image indicates the direction of movement of the disk from right to left.

0.05. At 294.0 s, the friction coefficient returned to a high value of 0.20 after the GO aggregates passed through the friction interface. The displacement between the ball and disk surfaces increased when the GO aggregates entered the friction interface. When the displacement was greater than approximately 40 nm, the friction coefficient attained the lowest value of 0.05.

The friction coefficient of GOA1 (whose density was 10 mass %) was investigated with a load of 0.8 mN using the microtribometer. The friction interface was observed using an optical microscope. Figure 9 depicts the friction coefficient (upper graph) and optical microscope images (middle graphs) of the microtribological test. During the run-in period, the friction coefficient was 0.075. The image during that time (4.03 s) reveals that the ball was slightly visible, which indicates the presence of a thick GO aggregate at the friction interface between the ball and plate surfaces. Then, the friction coefficient reached a maximum value of 0.11 and decreased rapidly. At that point, the ball began to appear, as shown in the microscopic image (7.14 s). This indicates that the thickness of the GO aggregates decreased owing to friction. After some time, the friction coefficient was less than 0.03. The microscope image (254.08 s) shows that the visible range of the ball increases, indicating that the thickness of the GO aggregates decreases. Interference fringes were not observed, which suggests that the GO aggregates remained near the friction interface and prevented their formation. We assumed the friction model of the GO aggregates, the schematic of which is shown in Figure 9. First, the direction of the GO layers in the GO aggregates was random, and it was considered to be resistant to friction. During friction, the thickness of the GO aggregates decreased, and the GO layers were aligned by the high pressure and shear stress of friction. The friction was considered to decrease because of the sliding between the layers with the smallest shear force in the multilayers. Under a macro load, the GO aggregates were pressed and sheared by

https://doi.org/10.1021/acsomega.2c04181
ACS Omega 2022, 7, 40983−40989

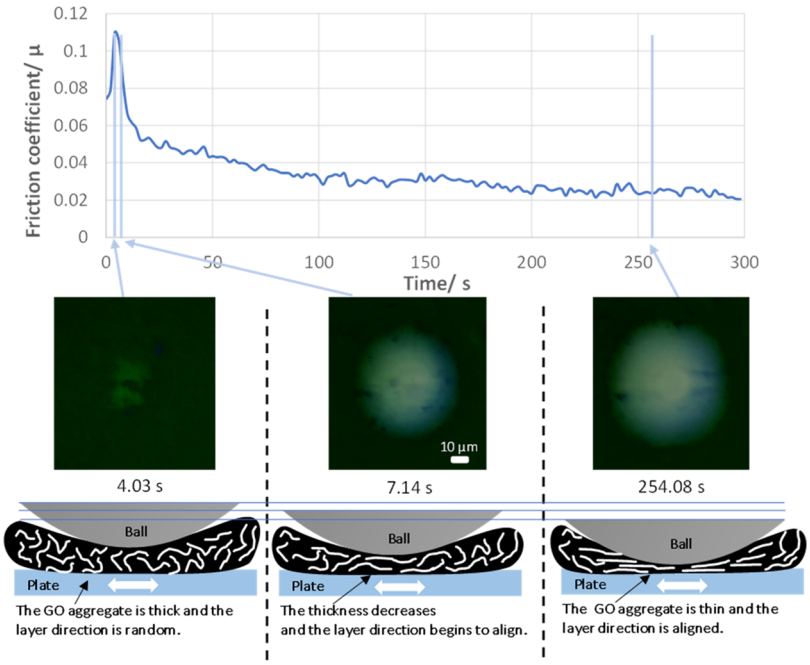

Figure 9. Friction coefficient (upper graph), optical microscope images (middle graphs), and schematic drawing of the assumed model (lower graphs) when the GO aggregates passed through the friction interface during the microtribological test.

the high-load friction when they entered the friction interface; thus, they were immediately aligned.

The low-spike friction of the GO aggregates formed by alkylamine was found to be lower than that formed by heating. It is assumed that because the GO aggregates formed by alkylamine possessed alkyl chains on the surfaces, which caused lower cohesive forces, they had a lower frictional force than the GO aggregates formed by heating.

Although the high-dispersible GO-dispersed PAO possessed lower friction coefficients than the pure PAO, its friction coefficient was only 0.15. It is considered that the isolated GO and/or small GO aggregates, not observed by optical microscopy, entered the friction interface. However, they could not fully cover the interfaces, and even if they fully covered them, the number of GO layers was very small.

4. SUMMARY

In this study, GO-dispersed PAOs with high and low dispersibility were synthesized. The low-dispersibility GO had high concentrations of oxygen functional groups. Friction tests were conducted using a ball-on-disk-type tribometer and microtribometer with an optical microscope. Many GO aggregates were found in the low-dispersible GO-dispersed PAO, which arose from the high concentrations of the oxygen functional groups. These aggregates occasionally entered and covered the friction interface. The frictional force was low only at that particular time. Especially the frictional coefficient of the GO aggregates formed by alkylamine had the lowest value of 0.05 because they covered the contact area completely. The microtribological test suggested that the thick GO aggregates had relatively high friction owing to the random directions of the GO layers, whereas the aligned direction of the GO layers had low friction. Therefore, in the macro-load tests, the directions of the GO layers were immediately aligned by the high-load friction, which leads to low friction. In contrast, for the high-dispersible GO-dispersed PAO, it was assumed that there were only a few GO layers at the friction interface, which had little effect on reducing friction.

■ ASSOCIATED CONTENT

Supporting Information

The Supporting Information is available free of charge at https://pubs.acs.org/doi/10.1021/acsomega.2c04181.

XPS C 1s, FTIR, and Raman spectra of GOA4, GOA10, GOT200, and GOT250, and optical microscope images between the ball and disk surfaces using GOA1, GOA4, GOA10, GOT130, GOT200, and GOT250 (PDF)

■ AUTHOR INFORMATION

Corresponding Author

Hiroshi Kinoshita − *Department of Mechanical Engineering, Graduate School of Engineering, University of Hyogo, Himeji 671-2280, Japan*; orcid.org/0000-0002-4439-9362; Email: kinoshita@eng.u-hyogo.ac.jp

Authors

Tatsuya Okamoto − *Department of Mechanical Engineering, Graduate School of Engineering, University of Hyogo, Himeji 671-2280, Japan*

Yutaro Hirai − *Department of Mechanical Engineering, Graduate School of Engineering, University of Hyogo, Himeji 671-2280, Japan*

Koichi Sugano − *Department of Mechanical Engineering, Graduate School of Engineering, University of Hyogo, Himeji 671-2280, Japan*

Matsumoto Naohiro − *Department of Mechanical Engineering, Graduate School of Engineering, University of Hyogo, Himeji 671-2280, Japan*

Complete contact information is available at: https://pubs.acs.org/10.1021/acsomega.2c04181

https://doi.org/10.1021/acsomega.2c04181
ACS Omega 2022, 7, 40983−40989

Author Contributions

H.K. and M.N. conceived the idea of the study and planned this study. H.K. made the frictional facility. M.N. conducted the measurements and analyses of XPS, FTIR, and Raman. T.O. and K.S. conducted the microtribological tests and their data analyses. Y.H. conducted the macrotribological tests and the data analyses. All authors reviewed the manuscript draft and revised it critically on intellectual content. All authors approved the final version of the manuscript to be published.

Notes

The authors declare no competing financial interest.

■ ACKNOWLEDGMENTS

This research was partly supported by grants from the Grants-in-Aid for Scientific Research (B) (17H03165, 20H02057).

■ REFERENCES

(1) Zhao, J.; Li, Y.; Wang, Y.; Mao, J.; He, Y.; Luo, J. Mild Thermal Reduction of Graphene Oxide as a Lubrication Additive for Friction and Wear Reduction. *RSC Adv.* **2017**, *7*, 1766−1770.

(2) Ismail, N. A.; Bagheri, S. Highly Oil-Dispersed Functionalized Reduced Graphene Oxide Nanosheets as Lube Oil Friction Modifier. *Mater. Sci. Eng. B* **2017**, *222*, 34−42.

(3) Zhang, L.; Sun, X.; Liu, X.; He, Y.; Chen, Y.; Liao, Z.; Gao, H.; Wang, S. Alkyl Titanate-Modified Graphene Oxide as Friction and Wear Reduction Additives in PAO Oil. *ACS Omega* **2021**, *6*, 3840−3846.

(4) Wang, W.; Zhang, G.; Xie, G. Ultralow Concentration of Graphene Oxide Nanosheets as Oil-Based Lubricant Additives. *Appl. Surf. Sci.* **2019**, *498*, No. 143683.

(5) Li, X.; Gan, C.; Han, Z.; Yan, H.; Chen, D.; Li, W.; Li, H.; Fan, X.; Li, D.; Zhu, M. High Dispersivity and Excellent Tribological Performance of Titanate Coupling Agent Modified Graphene Oxide in Hydraulic Oil. *Carbon* **2020**, *165*, 238−250.

(6) Cheng, Z. L.; Li, W.; Wu, P. R.; Liu, Z. A Strategy for Preparing Modified Graphene Oxide with Good Dispersibility and Transparency in Oil. *Ind. Eng. Chem. Res.* **2017**, *56*, 5527−5534.

(7) Zhang, W.; Zhou, M.; Zhu, H.; Tian, Y.; Wang, K.; Wei, J.; Ji, F.; Li, X.; Li, Z.; Zhang, P.; Wu, D. Tribological Properties of Oleic Acid-Modified Graphene as Lubricant Oil Additives. *J. Phys. D: Appl. Phys.* **2011**, *44*, No. 205303.

(8) Dou, X.; Koltonow, A. R.; He, X.; Jang, H. D.; Wang, Q.; Chung, Y.-W.; Huang, J. Self-Dispersed Crumpled Graphene Balls in Oil for Friction and Wear Reduction. *Proc. Natl. Acad. Sci. U.S.A.* **2016**, *113*, 1528−1533.

(9) Mungse, H. P.; Khatri, O. P. Chemically Functionalized Reduced Graphene Oxide as a Novel Material for Reduction of Friction and Wear. *J. Phys. Chem. C* **2014**, *118*, 14394−14402.

(10) Zhang, G.; Xu, Y.; Xiang, X.; Zheng, G.; Zeng, X.; Li, Z.; Ren, T.; Zhang, Y. Tribological Performances of Highly Dispersed Graphene Oxide Derivatives in Vegetable Oil. *Tribol. Int.* **2018**, *126*, 39−48.

(11) Alias, A. A.; Kinoshita, H.; Nishina, Y.; Fujii, M. Dependence of PH Level on Tribological Effect of Graphene Oxide as an Additive in Water Lubrication. *Int. J. Automot. Mech. Eng.* **2016**, *13*, 3150−3156.

(12) Kinoshita, H.; Nishina, Y. Investigations on Tribological Mechanisms of Graphene Oxide and Oxidized Wood-Derived Nanocarbons as Water-Based Lubricating Additives. *Tribol. Online* **2016**, *11*, 235−241.

(13) Kinoshita, H.; Ono, H.; Alias, A. A.; Nishina, Y.; Fujii, M. Tribological Properties of Graphene Oxide as a Lubricating Additive in Water and Lubricating Oils. *Mech. Eng. J.* **2015**, *2*, No. 15-00323.

(14) Kinoshita, H.; Nishina, Y.; Alias, A. A.; Fujii, M. Tribological Properties of Monolayer Graphene Oxide Sheets as Water-Based Lubricant Additives. *Carbon* **2014**, *66*, 720−723.

(15) Dreyer, D. R.; Park, S.; Bielawski, C. W.; Ruoff, R. S. The Chemistry of Graphene Oxide. *Chem. Soc. Rev.* **2010**, *39*, 228−240.

(16) Paredes, J. I.; Villar-Rodil, S.; Martínez-Alonso, A.; Tascón, J. M. D. Graphene Oxide Dispersions in Organic Solvents. *Langmuir* **2008**, *24*, 10560−10564.

(17) Zhao, J.; Huang, Y.; He, Y.; Shi, Y. Nanolubricant Additives: A Review. *Friction* **2021**, *9*, 891−917.

(18) Kinoshita, H.; Shibata, M.; Matsumoto, N. Entry Behavior into Friction Interface and Forming Unstable Lubricating Accumulation of Graphene Oxide between SUJ2 Ball and Glass Disk under Boundary Lubrication. *Tribol. Online* **2020**, *15*, 150−153.

(19) Chauveau, V.; Mazuyer, D.; Dassenoy, F.; Cayer-Barrioz, J. In Situ Film-Forming and Friction-Reduction Mechanisms for Carbon-Nanotube Dispersions in Lubrication. *Tribol. Lett.* **2012**, *47*, 467−480.

(20) Yang, D.; Velamakanni, A.; Bozoklu, G.; Park, S.; Stoller, M.; Piner, R. D.; Stankovich, S.; Jung, I.; Field, D. A.; Ventrice, C. A.; Ruoff, R. S. Chemical Analysis of Graphene Oxide Films after Heat and Chemical Treatments by X-Ray Photoelectron and Micro-Raman Spectroscopy. *Carbon* **2009**, *47*, 145−152.

(21) Chouhan, A.; Kumari, S.; Sarkar, T. K.; Rawat, S. S.; Khatri, O. P. Graphene-Based Aqueous Lubricants: Dispersion Stability to the Enhancement of Tribological Properties. *ACS Appl. Mater. Interfaces* **2020**, *12*, 51785−51796.

(22) Faniyi, I. O.; Fasakin, O.; Olofinjana, B.; Adekunle, A. S.; Oluwasusi, T. V.; Eleruja, M. A.; Ajayi, E. O. B. The Comparative Analyses of Reduced Graphene Oxide (RGO) Prepared via Green, Mild and Chemical Approaches. *SN Appl. Sci.* **2019**, *1*, No. 1181.

(23) Aziz, M.; Halim, F. S. A.; Jaafar, J. Preparation and Characterization of Graphene Membrane Electrode Assembly. *J. Teknol.* **2014**, *69*, 11−14.

(24) Emiru, T. F.; Ayele, D. W. Controlled Synthesis, Characterization and Reduction of Graphene Oxide: A Convenient Method for Large Scale Production. *Egypt. J. Basic Appl. Sci.* **2017**, *4*, 74−79.

(25) Ossonon, B. D.; Bélanger, D. Synthesis and Characterization of Sulfophenyl-Functionalized Reduced Graphene Oxide Sheets. *RSC Adv.* **2017**, *7*, 27224−27234.

(26) Andrijanto, E.; Shoelarta, S.; Subiyanto, G.; Rifki, S. In *Facile Synthesis of Graphene from Graphite Using Ascorbic Acid as Reducing Agent*; AIP Conference Proceedings: AIP Publishing, 2016.

https://doi.org/10.1021/acsomega.2c04181
ACS Omega 2022, 7, 40983−40989